Semiconductor Physics, Quantum Electronics & Optoelectronics, 2025. V. 28, No 3. P. 329-334.

Optics

EPR evidence of paramagnetic to spin glass transition in $Zn_{1-x}Mn_xSe:Fe^{2+}$ single crystals

A.V. Uriadov[1], I.V. Ivanchenko[2], N.A. Popenko[2], B.E. Bekirov[2], E.N. Kalabukhova[3], V.M. Tkach[4], D.V. Savchenko[1,5,*]

[1]*National Technical University of Ukraine "Igor Sikorsky Kyiv Polytechnic Institute" 37, prosp. Beresteiskyi, 03056 Kyiv, Ukraine*
[2]*O. Usikov Institute for Radiophysics and Electronics, NAS of Ukraine, 12, Proskura str., 61085 Kharkiv, Ukraine*
[3]*V. Lashkaryov Institute of Semiconductor Physics, NAS of Ukraine, 41, prosp. Nauky, 03028 Kyiv, Ukraine*
[4]*V. Bakul Institute for Superhard Materials, NAS of Ukraine, 2, Avtozavodskaya str., 04074 Kyiv, Ukraine*
[5]*Technical Center NAS of Ukraine, 13 Pokrovs'ka str., 04070 Kyiv, Ukraine*
[*]*Corresponding author e-mail: dariyasavchenko@gmail.com*

Abstract. In this work, the paramagnetic-to-spin glass transition in $Zn_{1-x}Mn_xSe:Fe^{2+}$ single crystals by using the analysis of temperature-dependent electron paramagnetic resonance (EPR) spectra were investigated. The transition is characterized by the broadening and a decrease in the amplitude of a single Lorentzian resonance line at $g \sim 2.01$, with critical freezing temperatures T_f at approximately 5.7 K for $x = 0.2$ and 8.0 K for $x = 0.3$. At lower temperatures, EPR spectra reveal three distinct paramagnetic centers attributed to Fe^{3+} ions at $g \sim 4.3$, strongly interacting Fe ions at $g \sim 2.05$, and a vacancy-type center at $g \sim 2.003$. These results indicate that iron doping promotes Mn clustering and stabilizes the spin glass phase, affecting the magnetic properties of $Zn_{1-x}Mn_xSe$.

Keywords: EPR, iron, zinc manganese selenide, spin glass transition.

https://doi.org/10.15407/spqeo28.03.329
PACS 61.82.Fk, 75.50.Pp, 76.30.Da, 76.30.-v

Manuscript received 06.04.25; revised version received 18.07.25; accepted for publication 03.09.25; published online 24.09.25.

1. Introduction

Diluted magnetic semiconductors (DMS), doped by magnetic ions (manganese (Mn), iron (Fe), or copper), reveal semiconducting and magnetic features, making them important for spintronics, where electron spin and charge are controlled for advanced data processing and storage applications [1]. DMS materials are promising for creating high-density, energy-efficient devices, *e.g.,* magnetic sensors and magnetic random-access memory (MRAM), which are increasingly critical in modern electronics [2].

The ability to control magnetic interactions in DMS systems, driven by superexchange and spin-orbit coupling, facilitates the stability crucial for developing reliable spin-based devices [3]. Moreover, DMS materials allow optical and magnetic manipulation, making them highly suitable for integrating optoelectronic devices that combine photonic and spintronic functions, particularly valuable in telecommunications and quantum computing applications.

Zinc manganese selenide ($Zn_{1-x}Mn_xSe$) is a widely studied DMS in which Mn ions replace zinc (Zn) ions in the crystal lattice of ZnSe. Embedding Mn ions into ZnSe creates localized magnetic moments, leading to a range of magnetic states depending on the temperature and Mn concentration [4]. Moreover, localized magnetic ions in $Zn_{1-x}Mn_xSe$ induce an exchange interaction between the *sp*-band electrons and the *d*-electrons associated with Mn^{2+}, leading to Zeeman splitting [5–7]. $Zn_{1-x}Mn_xSe$ can manifest paramagnetic, spin glass, or even antiferromagnetic behavior based on the Mn content and the interactions between the ions [8, 9]. These complex magnetic phases make $Zn_{1-x}Mn_xSe$ an ideal system for studying DMS material properties and understanding the effect of magnetic interactions on semiconductor properties.

Adding Fe^{2+} ions to the $Zn_{1-x}Mn_xSe$ matrix further enriches its magnetic and optical characteristics and increases the complexity of the magnetic interactions in the crystal [10]. $Zn_{1-x}Mn_xSe:Fe^{2+}$ material also shows potential for mid-infrared laser applications due to Fe^{2+} ions' strong fluorescence within the 4–6 μm range [11–13]. This combination of magnetic and optical properties in $Zn_{1-x}Mn_xSe:Fe^{2+}$ makes it a promising candidate for optoelectronic applications, where magnetic control over light properties is advantageous. The Fe-doping can also lead to spin-glass behavior in $Zn_{1-x}Mn_xSe$.

Electron paramagnetic resonance (EPR) is a helpful method for studying the magnetic properties of DMS. With the EPR technique, one can observe the behavior of magnetic ions under an external magnetic field and the subsequent temperature-dependent changes in their spin dynamics. Besides, by using the EPR spectroscopy, the paramagnetic-to-spin glass transition can be monitored by observing shifts in resonance signals and changes in linewidth, which indicate slowing spin dynamics and the onset of spin freezing.

This paper presents a detailed EPR analysis of $Zn_{1-x}Mn_xSe:Fe^{2+}$ single crystals, with a focus on the temperature-dependent evolution of the EPR spectra that allowed us to identify the transition from paramagnetic to spin glass state. Our study examines the broadening and amplitude changes of the single Lorentzian EPR line at higher temperatures and identifies distinct magnetic centers attributed to Fe^{3+} ions and Mn clusters, which appear at low temperatures. These findings provide detailed insight into the mechanisms of Fe-stimulated changes in magnetic interactions and the spin glass phase stabilization, advancing the understanding of dopant effects in DMS.

2. Materials and methods

According to [14], $Zn_{1-x}Mn_xSe$ crystals exhibit a zinc blende structure (with the stacking order ABCABC... along the [111] direction) for $x \le 0.30$ and a wurtzite structure (having ABABAB ... stacking along the c axis) for $x \ge 0.33$. Fig. 1 shows a typical zinc blend structure for $Zn_{1-x}Mn_xSe$ crystal. It is expected that Fe^{2+} ions substitute Zn^{2+} ions in $Zn_{1-x}Mn_xSe:Fe^{2+}$ crystal lattice [13].

In this work, $Zn_{1-x}Mn_xSe$ crystals with $x = 0.2$, 0.3, doped with divalent iron (Fe^{2+}) during the synthesis process, were grown using the Bridgman technique, as reported in [13].

The Mn concentrations of $x = 0.2$, 0.3 were chosen to provide the cubic phase of the crystals. The crystal samples were cut from the boule, and two surfaces were polished to laser grade. The crystal faces did not have any antireflection coatings. The same Fe^{2+} doping level in the melt at the level of $\sim 10^{19}$ cm^{-3} was kept for all crystals.

The microanalysis of the samples was performed using a scanning electron microscope ZEISS EVO 50XVP with a combined system of the energy-dispersion analysis INCA ENERGY 450 and structural HKL Channel 5 analysis. We used the operational mode of the spectrometer so that the analyzed surface area of the sample was <1 μm.

The atomic composition analysis was carried out on different sections of each crystal. For the sample with $x = 0.2$, the Mn concentration varied from 7.55 to 13.39 at.%, with Fe present in trace amounts up to 0.16 at.%, while Zn content was observed within the range of 34.86 to 19.23 at.%, and Se ranged from 73.22 to 51.59 at.%.

For the samples with $x = 0.3$, Mn concentration remained consistent between 12.80 and 12.68 at.%, with trace Fe levels reaching up to 0.18 at.%, whereas Zn was measured between 35.92 and 35.21 at.%, and Se ranged from 52.00 to 51.39 at.%. The observed variation in elemental percentages reflects heterogeneity across different crystal parts.

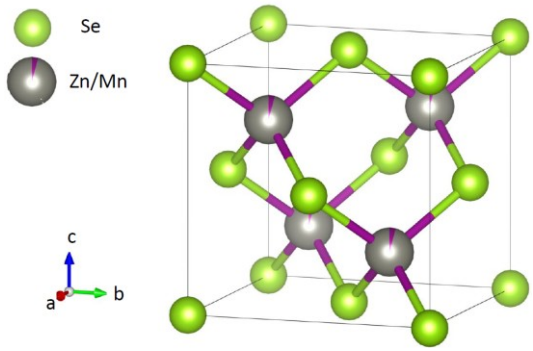

Fig. 1. Typical zinc blend crystal structure for $Zn_{1-x}Mn_xSe$ ($x = 0.05$) drawn in the VESTA 3.5.2 program [15] using the data from [14]. The $\vec{c}$ axis is parallel to the [001] direction.

Continuous wave EPR measurements were performed at the X-band frequency range (~9.4 GHz) using a Bruker ELEXSYS EPR E580 spectrometer with an ER 4112HV variable temperature helium-flow cryostat. Low-temperature EPR measurements were done on the SAFMAT research infrastructure (Institute of Physics of the Czech Academy of Sciences, Prague, Czech Republic). EPR measurements were performed using an ER 4122 SHQE SuperX High-Q cavity with the following experimental parameters: microwave power of 0.4743 mW, modulation frequency of 100 kHz, modulation amplitude of 0.8 mT, conversion time of 60 ms, and spectral resolution of 4096 points. A standard DPPH free radical with $g = 2.0036$ was used as a reference sample. The EPR spectra were simulated by the EasySpin 5.2.36 software package [16] using the 'pepper' function.

3. Results and discussion

The EPR spectra of $Zn_{1-x}Mn_xSe:Fe^{2+}$ crystals within the range 292…60 K consisted of a broad single isotropic Lorentzian line with $g \sim 2.01$ (see Fig. 2). The linewidth broadens and the amplitude of this signal decreases with decreasing temperature.

Fig. 3 reveals the temperature dependence of the peak-to-peak width (ΔB_{pp}) for this broad single Lorentzian line in $Zn_{1-x}Mn_xSe:Fe^{2+}$ crystals within the temperature range 300…10 K, obtained by simulating EPR spectra shown in Fig. 2.

Similar behavior for a single broad EPR line was previously observed in magnetically dilute $Cd_{1-x}Mn_xS$ semiconducting crystals with $x \ge 0.8$ [17] and $Zn_{1-x}Mn_xIn_2Se_4$ with $0.35 \le x \le 9$ [18, 19], and it was attributed to the strong exchange coupling between the Mn^{2+} ions [20]. In the solid solution compounds, the statistical fluctuations in concentrations lead to formation of microscopic regions with different Mn concentrations, so the Mn^{2+} ions are randomly distributed [19].

According to [21], the temperature decrease leads to more magnetically correlated spins within these regions, and as a result, the Mn magnetic clusters are formed.

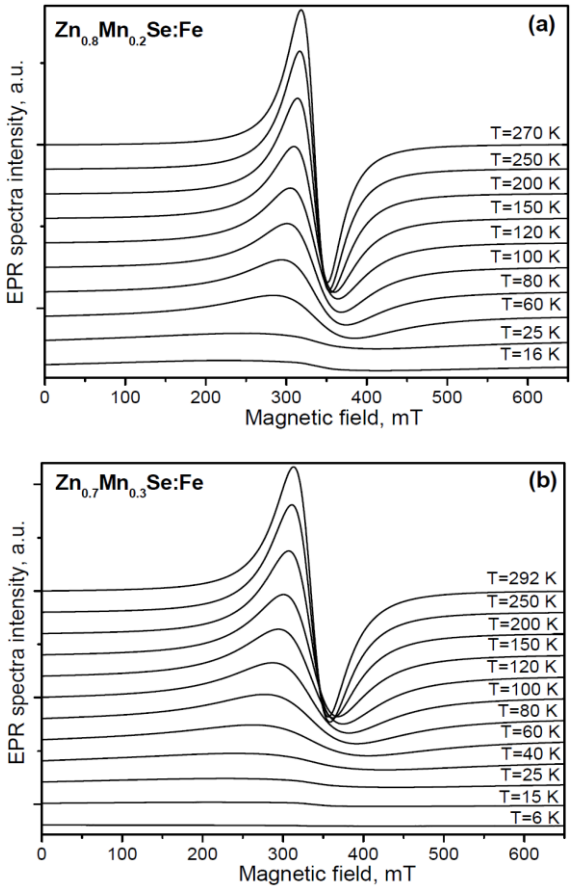

Fig. 2. Temperature dependence of X-band EPR spectra measured in $Zn_{1-x}Mn_xSe:Fe^{2+}$ crystals with $x = 0.2$ (a) and $x = 0.3$ (b).

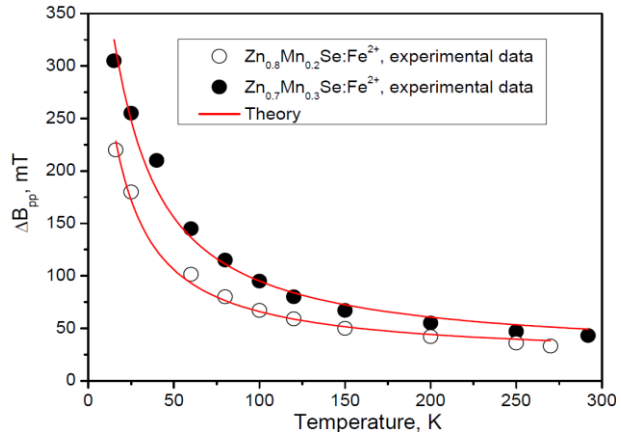

Fig. 3. Temperature dependence of linewidth for broad EPR signal at $g \sim 2.01$, obtained by simulation of EPR spectra temperature dependence, measured in $Zn_{1-x}Mn_xSe:Fe^{2+}$ crystals with $x = 0.2$ (open circles), and $x = 0.3$ (filled circles) presented in Fig. 2. Solid red lines – the result of the fitting of experimental data with Eq. (1).

The fact that the broad single EPR line becomes slightly asymmetric can be explained by the increase in the dilution of magnetic ions and formation of the isolated domain of Mn ions [22].

According to [23], the temperature dependence of the linewidth of the broad EPR signal shown in Fig. 3 can be described as:

$$\Delta B(T) = \Delta B_\infty \left(1 - \Theta / T\right) \exp\left(-jT_f / T\right), \qquad (1)$$

where ΔB_∞ is the linewidth of the signal at very high temperatures, Θ is the Curie temperature, j is equal to +1 for a micromagnetic (spin glass) system and –1 for the case of antiferromagnetic ordering, and T_f is the freezing or Néel temperature.

The first part of Eq. (1) is related to the paramagnetic behavior of the system [24], whereas the exponential factor is associated with the inverse relaxation time proportional to the EPR linewidth [25].

The parameters obtained by fitting Eq. (1) with experimental data shown in Fig. 3 are represented in the table. The obtained Θ values are close to those reported in [26] for $Zn_{0.7}Mn_{0.3}Se$ ($\Theta = -280.3$ K). The T_f values are close to $T_f = 5.7$ K determined in $Zn_{0.755}Mn_{0.245}Se$ [9]. In our samples, the $j = 1$ value corresponds to the phase transition from the paramagnetic phase to the spin glass at the critical temperature T_f within the 5.7…8 K range.

At $T < 60$ K, an additional line with $g \sim 1.99$ and linewidth of $\Delta B_{pp} \sim 70$ mT appears in EPR spectra of $Zn_{1-x}Mn_xSe:Fe^{2+}$ crystals (Fig. 4). The coexistence of two broad lines in EPR spectra of $Cd_{1-x}Mn_xTe$ and $Zn_{1-x}Mn_xTe$ compounds was previously explained by the formation of Mn clusters of two types: larger clusters (broader EPR line) and smaller ones (narrower EPR line) [27]. Thus, the EPR line at $g \sim 1.99$ can be tentatively attributed to the formation of Mn clusters of small size.

As can be seen from Fig. 4, the transition from the paramagnetic phase to the spin glass one at T_f is accompanied by the disappearance of two broad EPR lines, while three less intense and narrower isotropic EPR signals appear at $g \sim 4.3$ ($\Delta B_{pp} \sim 4.4$ mT), $g \sim 2.05$ ($\Delta B_{pp} \sim 9.7$ mT), and $g \sim 2.003$ ($\Delta B_{pp} \sim 1.1$ mT).

It is well known that Fe^{3+} ions have a d configuration with ^6S as the free ion ground state without spin-orbit interaction [28], and its g-factor value is expected to be close to the free-electron value ($g_e \sim 2.0023$). Though a g-factor much higher than g_e often occurs, increasing when certain symmetry elements are present [29]. If Fe^{3+} ions are in a crystal field environment, the ^6S ground state splits into three Kramer's doublets $|\pm 1/2\rangle$, $|\pm 3/2\rangle$ and $|\pm 5/2\rangle$, and the resonance signal at $g \sim 4.2$ corresponds to the middle Kramer's doublet $|\pm 3/2\rangle$ [30]. Thus, the observed EPR line at $g \sim 4.3$ should be attributed to Fe^{3+} ions at distorted tetrahedral symmetry sites.

Table. The parameters obtained for $Zn_{1-x}Mn_xSe:Fe^{2+}$ crystals by fitting Eq. (1) with experimental data shown in Fig. 3.

x	ΔB_∞, mT	Θ, K	T_f, K	j
0.2	21.0	–232.7	5.7	1
0.3	23.3	–341.8	8.0	1

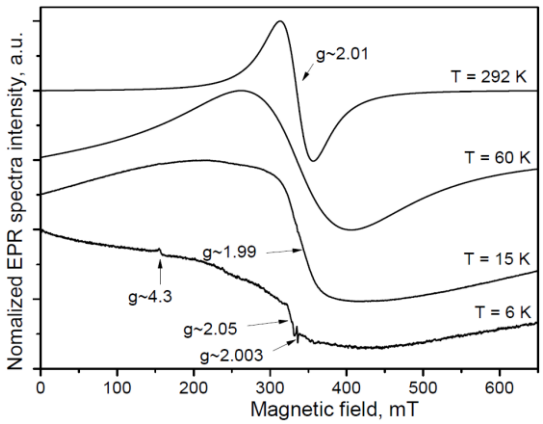

Fig. 4. EPR spectra measured at temperatures higher and lower than $T_f = 8$ K for $Zn_{1-x}Mn_xSe:Fe^{2+}$ crystals with $x = 0.3$. The EPR spectra intensity was normalized to its maximum value.

The linewidth of the EPR signal at $g \sim 2.05$ is 9.7 mT, so it cannot be assigned to the Mn-related center having a hyperfine splitting constant of ~ 6.0 mT and undergoing a broadening effect at high Mn content. Thus, this EPR signal may be caused by strongly interacting Fe^{3+} ions. The narrow line at $g \sim 2.003$ can be assigned to a vacancy-type center (probably a zinc one).

It should be noted that we did not observe the EPR signals from Fe^{2+} ions, which can be explained by the fact that Fe^{2+} ($3d^6$ configuration) in a tetrahedral crystal field, like in $Zn_{1-x}Mn_xSe$, is expected to be in a high-spin state with no net magnetic moment, leading to an $S = 0$ state in its ground configuration [31]. As a result, Fe^{2+} does not produce a detectable EPR signal under typical conditions. On the other hand, Fe^{3+} ions are also more prone to be stabilized in specific environments within the crystal due to oxidation processes, which might contribute to the prevalence of Fe^{3+} signals in the EPR spectra in $Zn_{1-x}Mn_xSe:Fe^{2+}$ crystals.

4. Conclusions

This work presents a comprehensive EPR analysis of $Zn_{1-x}Mn_xSe:Fe^{2+}$ single crystals with $x = 0.2$ and $x = 0.3$, providing new insights into the magnetic interactions occurring within this DMS system. Our analysis revealed a pronounced temperature dependence of the single Lorentzian EPR line at $g \sim 2.01$, which broadens and diminishes in amplitude as the temperature decreases. This behavior indicates the slowing spin dynamics that precede the spin freezing process, marking the transition from a paramagnetic to a spin glass phase. The critical freezing temperatures observed approximately at ~ 5.7 K for $x = 0.2$, and ~ 8.0 K for $x = 0.3$ demonstrate the influence of Mn concentration on the stability of the magnetic phases.

The emergence of an additional EPR line with $g \sim 1.99$ at $T < 60$ K reflects the formation of small Mn clusters within the $Zn_{1-x}Mn_xSe:Fe^{2+}$ matrix.

At temperatures below the spin glass transition, the EPR spectra exhibit several signals. The first center, observed at $g \sim 4.3$, is attributed to Fe^{3+} ions in crystal sites with distorted tetrahedral symmetry. The second center, with a signal at $g \sim 2.05$, corresponds to strongly interacting Fe ions, reflecting regions of high local magnetic concentration. Finally, a third narrow line at $g \sim 2.003$ likely arises from a vacancy-type center, possibly associated with zinc vacancies, which further influences the magnetic phase at low temperatures. These findings establish $Zn_{1-x}Mn_xSe:Fe^{2+}$ as a valuable model for studying spin glass behavior in DMS. The insights gained from this work could be important for future developments in spintronic applications, where controlled magnetic states are essential for advancing device functionality.

Acknowledgments

The authors are grateful to Dr. N. Kovalenko (Helmut Schmidt University, Hamburg, Germany) for supplying samples for the study.

References

1. Baruah J.M., Narayan J. Dilute magnetic semiconducting quantum dots: Smart materials for spintronics, Chap. 11 in: *Nonmagnetic and Magnetic Quantum Dots*, Ed. V. Stavrou. IntechOpen, London, UK, 2018. P. 187–199. https://doi.org/10.5772/intechopen.73286.
2. Zhao G.Q., Deng Z., Jin C.Q. Advances in new generation diluted magnetic semiconductors with independent spin and charge doping. *J. Semicond*. 2019. **40**, No 8. P. 081505. https://doi.org/10.1088/1674-4926/40/8/081505.
3. Fan Y. Recent progress in diluted ferromagnetism for spintronic application. *J. Phys. Conf. Ser*. 2023. **2608**. P. 012046. https://doi.org/10.1088/1742-6596/2608/1/012046.
4. Xu S., Xu X., Wang C. *et al.* Theoretical and experimental investigation of doping M in ZnSe (M = Cd, Mn, Ag, Cu) clusters: optical and bonding characteristics. *Luminescence*. 2015. **31**, No 2. P. 312–316. https://doi.org/10.1002/bio.3056.
5. Imamura M., Tashima D., Kitagawa J., Asada H. Magneto-optical properties of wider gap semiconductors ZnMnTe and ZnMnSe films prepared by MBE. *JEST*. 2020. **18**, No 1. P. 100056. https://doi.org/10.1016/j.jnlest.2020.100056.
6. Twardowski A., von Ortenberg M., Demianiuk M., Pauthenet R. Magnetization and exchange constants in $Zn_{1-x}Mn_xSe$. *Solid State Commun*. 1984. **51**, No 11. P. 849–852. https://doi.org/10.1016/0038-1098(84)91085-8.
7. Sandratskii L.M. Exchange interactions in (ZnMn)Se: LDA and LDA+U calculations. *Phys. Rev. B*. 2003. **68**, No 22. P. 224432. https://doi.org/10.1103/PhysRevB.68.224432.
8. Furdyna J.K. Diluted magnetic semiconductors. *J. Appl. Phys*. 1988. **64**. P. R29–R64. https://doi.org/10.1063/1.341700.
9. Twardowski A., Denissen C.J.M., de Jonge W.J.M. *et al.* Spinglass behaviour of $Zn_{1-x}Mn_xSe$ and $Zn_{1-x}Mn_xTe$ semimagnetic semiconductors. *Phys. Rev. B*. 1987. **36**, No 12. P. 7013–7021. https://doi.org/10.1016/0038-1098(86)90579-X.

10. Doroshenko M.E., Osiko V.V., Jelinkova H. *et al.* Spectroscopic and laser properties of Fe^{2+} ions in solid solutions based on ZnSe crystal. In: *Proc. Advanced Solid State Lasers (ASSL) Conference*, 4–9 October 2015, Berlin, Germany, P. ATu2A.15. https://doi.org/10.1364/ASSL.2015.ATU2A.15.
11. Švejkar R., Šulc J., Jelínková H. *et al.* Compact Fe:ZnSe and Fe:ZnMnSe tunable lasers at 80 K pump with Er:YAG In: *Proc. 2018 Conf. on Lasers and Electro-Optics Pacific Rim (CLEO-PR)*, 29 July – 03 Aug. 2018, Hong Kong, China. P. W3A.55. https://doi.org/10.1364/CLEOPR.2018.W3A.55.
12. Jelínková H., Doroshenko M.E., Osiko V.V. *et al.* $Fe:Zn_{0.6}Mn_{0.4}Se$ spectroscopic properties and laser generation at 5.0–5.8 μm in the temperature range of 78–300 K. In: *Proc.2018 Conf. on Lasers and Electro-Optics Pacific Rim (CLEO-PR)*, Hong Kong, China, 2018. P. W3A.56. https://doi.org/10.1364/CLEOPR.2018.W3A.56.
13. Doroshenko M.E., Jelínková H., Osiko V.V. *et al.* Fe:ZnMnSe laser active material at 78–300 K: Spectroscopic properties and laser generation at 4.2–5.0 μm. *J. Lumin.* 2017. **192**. P. 1300–1307. https://doi.org/10.1016/j.jlumin.2017.09.014.
14. Yoder-Short D.R., Debska U., Furdyna J.K. Lattice parameters of $Zn_{1-x}Mn_xSe$ and tetrahedral bond lengths in $A^{II}{}_{1-x}Mn_xB^{VI}$ alloys. *J. Appl. Phys*. 1985. **58**, P. 4056–4060. https://doi.org/10.1063/1.335585.
15. Momma K., Izumi F. VESTA 3 for three-dimensional visualization of crystal, volumetric and morphology data. *J. Appl. Crystallogr.* 2011. **44**. P. 1272. https://doi.org/10.1107/S0021889811038970.
16. Stoll S., Schweiger A. EasySpin, a comprehensive software package for spectral simulation and analysis in EPR. *J. Magn. Reson*. 2006. **178**, No 1. P. 42–55. https://doi.org/10.1016/j.jmr.2005.08.013.
17. Goede O., Backs D., Heimbrodt W., Kanis M. EPR study of the antiferromagnetic phase transition in (Cd, Mn)S. *phys. status solidi (b)*. 1989. **151**, No 1. P. 311–318. https://doi.org/10.1002/pssb.2221510135.
18. Mantilla J.C., Pontuschka W.M., Gamarra L.F. *et al*. Magnetic resonance in the $Zn_{1-x}Mn_xIn_2Se_4$ dilute magnetic semiconductor system. *J. Phys. Condens. Matter*. 2005. **17**, No 17. P. 2755–2766. https://doi.org/10.1088/0953-8984/17/17/025.
19. Sagredo V., Silva P., Diaz M. *et al*. Magnetic behaviour of the semimagnetic semiconductor $Zn_{1-x}Mn_xIn_2Te_4$. *phys. status solidi (b)*. 2000. **220**, No 1. P. 237–241. https://doi.org/10.1002/1521-3951(200007)220:1<237::AID-PSSB237>3.0.CO;2-T.
20. Deigen M., Maevskii V., Potykevich I. *et al*. Study of the concentration dependence of the EPR of Mn^{2+} in CdTe single crystals. *Sov. Phys. Solid State*. 1967. **9**. P. 773–782.
21. Palacio F., Campo J., Sagredo V. *et al*. Magnetic characterization of the spin-glass phase in $Mn_xCd_{1-x}In_2Te_4$ solid solutions. *Mater. Sci. Forum*. 1995. **182-184**. P. 459–462. https://doi.org/10.4028/www.scientific.net/MSF.182-184.459.
22. Viticoli S., Fiorani D., Nogués M., Dormann J.L. Magnetic resonance of the insulating spin-glass spinel solid solution $CdCr_{2x}In_{2-2x}S_4$ ($0.25 \le x \le 0.85$). *Phys. Rev. B*. 1982. **26**. P. 6085. https://doi.org/10.1103/PhysRevB.26.6085.
23. Silva P., Fermin J., Chourio M. *et al*. EPR measurements on the $CuCd_{1-x}Mn_xGeSe_4$ diluted magnetic semiconductor. *Cryst. Res. Technol*. 1996. **31**. P. 569–573.
24. Oseroff S., Calvo R., Giriat W. Electron spin resonance in $Cd_{1-x}Mn_xTe$. *J. Appl. Phys*. 1979. **50**, No B11. P. 7738–7739. https://doi.org/10.1063/1.326806.
25. Oseroff S.B. Magnetic susceptibility and EPR measurements in concentrated spin-glasses: $Cd_{1-x}Mn_xTe$ and $Cd_{1-x}Mn_xSe$. *Phys. Rev. B*. 1982. **25**. P. 6584–6595. https://doi.org/10.1103/PhysRevB.25.6584.
26. Furdyna J.K., Samarth N., Frankel R.B., Spalek J. Static magnetic susceptibility of $Zn_{1-x}Mn_xSe$. *Phys. Rev. B*. 1988. **37**, No 7. P. 3707–3712. https://doi.org/10.1103/PhysRevB.37.3707.
27. Partyka J., Žukowski P.W., Wegierek P. *et al*. Electron spin resonance in $Cd_{1-x}Mn_xTe$ and $Zn_{1-x}Mn_xTe$ compounds. *Semiconductors.* 2002. **36**, No 12. P. 1347–1351. https://doi.org/10.1134/1.1529244.
28. Loveridge D., Parke S. Electron spin resonance of Fe^{3+}, Mn^{2+} and Cr^{3+} in glasses. *Phys. Chem. Glas*. 1971. **12**, No 1. P. 19–27.
29. Chakradhar R.P.S., Sivaramaiah G., Lakshmana Rao J., Gopal N.O. Fe^{3+} ions in alkali lead tetraborate glasses – an electron paramagnetic resonance and optical study. *Spectrochim. Acta A Mol. Biomol. Spectrosc*. 2005. **62**, Issues 1–3. P. 51–57. https://doi.org/10.1016/j.saa.2004.12.004.
30. Kliava J. EPR of impurity ions in disordered solids: distributions of the spin Hamiltonian parameters. *phys. status solidi (b)*. 1986. **134**, No 2. P. 411–455. https://doi.org/10.1002/pssb.2221340202.
31. Basu C., Ghosh U.S. Contribution of configuration interaction to the intensity of crystal field transitions in tetrahedral Fe^{2+} ion. *phys. status solidi (b)*. 1973. **60**, No 1. P. 97–106. https://doi.org/10.1002/pssb.2220600110.

Authors' contributions

Uriadov A.V.: formal analysis, data curation, writing – original draft.
Ivanchenko I.V.: conceptualization, writing – review & editing.
Popenko N.A.: methodology, validation, writing – review & editing.
Bekirov B.E.: data curation (partially), writing – original draft, visualization.
Kalabukhova E.N.: supervision, writing – review & editing.
Tkach V.M.: methodology, investigation.
Savchenko D.V.: methodology, investigation, software, formal analysis, data curation, writing – original draft, writing – review & editing.

Authors and CV

Andrii V. Uriadov, PhD Student at the Department of General Physics and Modelling of Physical Processes, National Technical University of Ukraine "Igor Sikorsky Kyiv Polytechnic Institute". The area of his scientific interests includes magnetic resonance in semiconductors and magnetic alloys.
E-mail: a.uriadov@kpi.ua,
https://orcid.org/0009-0008-8110-9505

Igor V. Ivanchenko, Doctor of Sciences in Radiophysics, Leading Researcher at the Radiospectroscopy Department, O. Usikov Institute for Radiophysics and Electronics, NASU. The area of his scientific interests includes radiospectroscopy of diluted semiconductors. E-mail: ivanchenkoi534@gmail.com,
https://orcid.org/0000-0003-2540-4995

Nina A. Popenko, Doctor of Sciences in Radiophysics, Leading Researcher at the Radiospectroscopy Department, O. Usikov Institute for Radiophysics and Electronics, NASU. The area of her scientific interests includes radiospectroscopy of diluted semiconductors.
E-mail: ireburan@yahoo.com

Bekir E. Bekirov, PhD, Researcher at the Radiospectroscopy Department, O. Usikov Institute for Radiophysics and Electronics, NASU. The area of his scientific interests includes radiospectroscopy of diluted semiconductors. E-mail: bekirbekirov1986@gmail.com

Ekaterina N. Kalabukhova, Doctor of Sciences in Physics and Mathematics, Leading Researcher at the Department of Semiconductor Heterostructures, V. Lashkaryov Institute of Semiconductor Physics, NASU. The area of her scientific interests includes magnetic resonance in semiconductor and nanosized materials.
E-mail: kalabukhova@yahoo.com,
https://orcid.org/0000-0003-0272-9471

Vasyl M. Tkach, Doctor of Sciences in Physics and Mathematics, Leading Researcher at the Laboratory of nanostructural and crystallophysical researches, V. Bakul Institute for Superhard Materials, NAS of Ukraine. His research interests include solid state physics, superhard materials, nanostructures and nanoscale materials, scanning electron microscopy.
E-mail: tkach@ism.kiev.ua

Dariya V. Savchenko, Doctor of Sciences in Physics and Mathematics, Head of the Department of General Physics and Modelling of Physical Processes of the National Technical University of Ukraine "Igor Sikorsky Kyiv Polytechnic Institute" and Senior Researcher at the Technical center, NAS of Ukraine. The area of her scientific interests includes magnetic resonance in semiconductors, dielectrics and biomaterials.
https://orcid.org/0000-0002-0005-0732

ЕПР підтвердження переходу парамагнетик-спінове скло у монокристалах $Zn_{1-x}Mn_xSe:Fe^{2+}$

А.В. Урядов, І.В. Іванченко, Н.А. Попенко, Б.Е. Бекіров, К.М. Калабухова, В.М. Ткач, Д.В. Савченко

Анотація. У цій роботі досліджується перехід від парамагнітного стану до стану спінового скла в монокристалах $Zn_{1-x}Mn_xSe:Fe^{2+}$ за допомогою аналізу температурно-залежних спектрів електронного парамагнітного резонансу (ЕПР). Перехід характеризується розширенням і зменшенням амплітуди одиночної резонансної лінії ЕПР Лоренцевої форми з $g \sim 2.01$, з критичними температурами замерзання T_f біля 5.7 K для $x = 0.2$ та 8.0 K для $x = 0.3$. За нижчих температур спектри ЕПР мають три відокремлені парамагнітні центри, пов'язані з іонами Fe^{3+} з $g \sim 4.3$, сильно взаємодіючими іонами Fe з $g \sim 2.05$ і центром вакансійного типу з $g \sim 2.003$. Ці результати вказують на те, що легування залізом сприяє кластеризації Mn і стабілізує фазу спінового скла, впливаючи на магнітні властивості $Zn_{1-x}Mn_xSe$.

Ключові слова: ЕПР, залізо, селенід цинку марганцю, перехід до стану спінового скла.